



Chaos in the quantum Duffing oscillator in the semiclassical regime under parametrized dissipation

Andrew D. Maris ^{1,2} Bibek Pokharel ^{3,*} Sharan Ganjam Seshachallam,¹
Moses Z. R. Misplon,¹ and Arjendu K. Pattanayak ¹

¹*Department of Physics and Astronomy, Carleton College, One North College Street, Northfield, Minnesota 55057, USA*

²*Department of Nuclear Science and Engineering, Massachusetts Institute of Technology,
77 Massachusetts Avenue, Cambridge, Massachusetts 02139, USA*

³*Department of Physics, University of Southern California, Los Angeles, California 90089, USA*



(Received 28 November 2020; revised 27 March 2021; accepted 2 June 2021; published 6 August 2021)

We study the quantum dissipative Duffing oscillator across a range of system sizes and environmental couplings under varying semiclassical approximations. Using spatial complexity metrics based on Kullback-Leibler distances between phase-space attractors and temporal complexity metrics based on the Lyapunov exponent, we isolate the effect of the environment on quantum-classical differences. Moreover, we quantify the system sizes where quantum dynamics cannot be simulated using semiclassical or noise-added classical approximations. We find that a remarkable parametrically invariant meta-attractor emerges at a specific length scale and noise-added classical models deviate strongly from quantum dynamics below this scale. We also generalize the previous surprising result that classically regular orbits can have the greatest quantum-classical differences in the semiclassical regime and show that the dynamical growth of quantum-classical differences is not determined by the degree of classical chaos.

DOI: [10.1103/PhysRevE.104.024206](https://doi.org/10.1103/PhysRevE.104.024206)

I. INTRODUCTION

Nonlinearity is a quantum-mechanical resource useful in amplifying quantum-classical differences [1]. Quantum systems at the length and energy scales of current experimental relevance are best treated as open to the environment and are thus termed NISQ (noisy intermediate scale quantum) systems [2]. These environmental effects lead to decoherence but can also be exploited through measurement feedback [3,4]. Experimentalists and theorists have both worked on understanding the transition between quantum and classical behavior in such nonlinear quantum dissipative systems (NQDS) [5–7]. Specifically, chaos, or sensitivity to initial conditions and parameters, in an NQDS is fundamentally different from Hamiltonian chaos and can be quantified using the Lyapunov exponent [8,9]. This has been further extended by several groups including Pokharel *et al.* [10], Eastman *et al.* [3], Yusipov *et al.* [11], and Ralph *et al.* [12]. These results have established that open nonlinear quantum systems have a smooth [13–20] but nonmonotonic [21] and rich quantum-to-classical transition. The details of the mechanism, including the role of the environment in this transition, have not been fully characterized.

In this context, we report on a study examining with care the effect of changing parameters on the complexity of the dynamics. We consider semiclassical approximations for the dissipative quantum Duffing oscillator that are derived from a quantum master equation under the assumption of a Markovian environment. We find that visual correspon-

dence between different phase-space Poincaré sections does not translate to them having equal Lyapunov exponent and vice versa. That is, the spatial and temporal complexity of the dynamics can be and are indeed found to be independent of each other (see Fig. 1). Therefore, we use a Kullback-Liebler distance between phase space attractors as well as the corresponding Lyapunov exponents to better characterize the different changes in complexity. Our results can be summarized as follows:

(1) The primary effect of decreasing length scales is seen to be an increasing sensitivity to environmental fluctuations. However, this behavior is not explained by the effects of adding Gaussian noise to the classical system. Such artificial noise-added classical systems reproduce some of the qualitative behavior of quantum noise temporally, but are measurably spatially different.

(2) At a certain length scale the environment washes out differences between classically chaotic and periodic trajectories. This leads to a chaotic meta-attractor which is invariant to changes in environmental coupling. For systems that are smaller than this length scale, noise-added classical models diverge significantly from the semiclassical dynamics.

(3) The deviation from the classical limit is maximal for those systems where the global attractor is a classical periodic orbit (PO). In other words, in keeping with previous results [10] these POs are more sensitive to environmental effects of changing length scales than classically chaotic orbits and quantum-classical correspondence requires larger length scales for POs than for chaos.

(4) In contrast to the standard intuition, even for chaotic systems the degree of classical chaos, i.e., the maximal classical Lyapunov exponent, is *not* correlated to the

*Corresponding author: bbk.pokharel@gmail.com

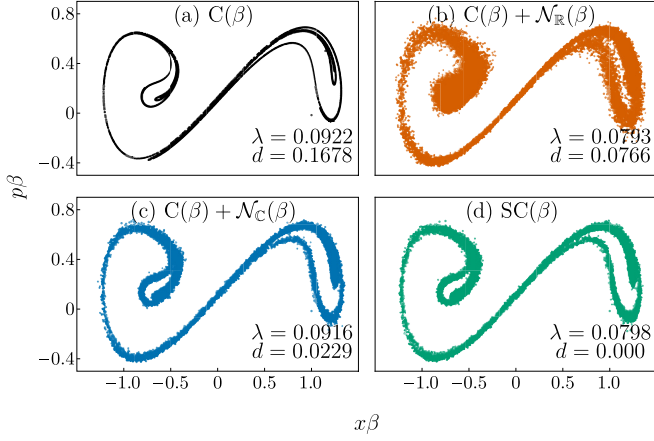


FIG. 1. Different approximations are compared to the semiclassical model. Chaotic attractors for the Duffing oscillator at a representative environmental coupling ($\Gamma = 0.174$) and system size ($\beta = \beta_{\text{conv}}$) are shown. The four figures are obtained under different semiclassical approximations described in more detail in the text. Note that while (c) and (d) are hard to distinguish visually, they are well separated using the Lyapunov exponent or the SKL measure. At the same time, attractors in (a) and (c), and (b) and (d) have the same Lyapunov exponent respectively. All four approximations have a unique distance d from SC, with cruder approximations appropriately having a larger d .

length scale where the classical and semiclassical dynamics deviate.

This careful consideration of Lyapunov exponents paired with the use of other measures thus reveals that the quantum to classical transition for NQDS is filled with a wealth of nonintuitive phenomena arising from the interplay between chaos, noise and quantum-effects at this scale. In what follows, we present our basic models and methods, before turning to results and a concluding discussion.

II. METHODS

The open quantum Duffing oscillator is a paradigmatic model to study quantum to classical transition for chaos. The Newtonian limit is a unit mass in a double-well potential with dissipation Γ , sinusoidal driving amplitude g , frequency ω , and dimensionless length scale β ,

$$\ddot{x} + 2\Gamma\dot{x} + \beta^2 x^3 - x = \frac{g}{\beta} \cos(\Omega t). \quad (1)$$

The quantum Duffing oscillator is described using Quantum State Diffusion theory [22] where the stochastic evolution of a single pure quantum system $|\psi\rangle$ under continuous measurement (including by the environment, for example) is considered. For this open system evolution, the Hamiltonian is

$$\hat{H} = \frac{1}{2}\hat{P}^2 + \frac{\beta^2}{4}\hat{Q}^4 - \frac{1}{2}\hat{Q}^2 + \frac{\Gamma}{2}(\hat{Q}\hat{P} + \hat{P}\hat{Q}) - \frac{g}{\beta}\hat{Q}\cos(\Omega t), \quad (2)$$

and dissipation due to coupling to the environment is represented by a single Lindblad operator $\hat{L} = \sqrt{\Gamma}(\hat{X} + i\hat{P})$ [23]. The corresponding Langevin-Ito equation for the evolution of

the wave function is then

$$|d\psi\rangle = -\frac{i}{\hbar}\hat{H}|\psi\rangle dt + (\hat{L} - \langle\hat{L}\rangle)|\psi\rangle d\xi + \left(\langle\hat{L}^\dagger\rangle\hat{L} - \frac{1}{2}\hat{L}^\dagger\hat{L} - \frac{1}{2}\langle\hat{L}^\dagger\rangle\langle\hat{L}\rangle\right)|\psi\rangle dt. \quad (3)$$

In this system, both the dissipation and the quantum nonlinearity scale with Γ , via \hat{L} . The stochastic nature of the dynamics arises from independent normalized complex differential random variables $d\xi$, where the mean M over realizations is $M(d\xi) = 0$, $M(d\xi d\xi) = 0$, $M(d\xi d\xi^*) = dt$.

This formulation of the Duffing oscillator has a single parameter $\beta \equiv \sqrt{\frac{\hbar}{I^2 m \omega}}$ that determines the scale of the system. The dynamics of Eq. (1) defines the ‘‘classical limit,’’ which is invariant under change in β except for change of the length scale. However, the dynamics of Eq. (3) do vary with β ; in particular Eq. (1) can be derived for the expectation values of the position \hat{X} , \hat{P} for the evolving $|\psi\rangle$ as $\beta \rightarrow 0$. Thus, this parameter allows us to study the transition [23,24] from the quantum scale $\beta \rightarrow 1$ to $\beta \rightarrow 0$, the largest length scales where the quantum predictions become scale invariant and agree identically with the Newtonian predictions; that is, β is a scaled Planck’s constant representing the level of ‘‘quantumness’’ of the system. It is possible to change the relative nonlinearity by changing the coefficient of the quartic or quadratic term in the Hamiltonian. Similarly we can change the amplitude and frequency of the driving independent of β of course. For our investigation, we focus on the effects of the environment by scanning over nontrivial damping $0 < \Gamma < 0.35$ with an interval of $\delta\Gamma = 0.002$ with other parameters fixed as $g = 0.3$, $\Omega = 1$ as in Ref. [10]. This yields a sufficiently rich regime of dynamics to study for our purposes.

Previous studies [25] and Pokharel *et al.* [10] use a semiclassical stochastic equation valid when the wave function is sufficiently sharply localized by the action of the environment. This allows the dynamics to be accurately tracked by studying the dynamics of the first- and second-order moments of the position and the momentum, $x = \langle\hat{X}\rangle$, $p = \langle\hat{P}\rangle$, $\mu = \sigma_{XX}$, $\kappa = \sigma_{PP}$, $R = \frac{1}{2}(\sigma_{XP} + \sigma_{PX})$ where $\sigma_{AB} = \langle(A^\dagger - \langle A \rangle^*)(B - \langle B \rangle)\rangle$. It is possible to reduce this system further—decreasing the number of variables in this stochastic differential equation (SDE) system from five to four (see Appendix A)—by observing a conserved quantity $\mu\kappa - R^2 = \frac{1}{4}$ and then making a change of variables $\mu = \rho^2$, $R = \rho\Pi$. This yields for the Duffing oscillator the semiclassical coupled SDEs

$$dx = p dt + 2\sqrt{\Gamma}\left[\left(\rho^2 - \frac{1}{2}\right)d\xi_R - \rho\Pi d\xi_I\right], \quad (4)$$

$$dp = \left[-\beta^2 x^3 + (1 - 3\beta^2 \rho^2)x - 2\Gamma p + \frac{g}{\beta} \cos(\omega t)\right] dt + 2\sqrt{\Gamma}\left[\rho\Pi d\xi_R - \left(\frac{1}{2} - \Pi^2 - \frac{1}{4\rho^2}\right)d\xi_I\right], \quad (5)$$

$$d\rho = \left[\Pi + \Gamma\left(\rho - \rho^3 - \rho\Pi^2 + \frac{1}{4\rho}\right)\right] dt, \quad (6)$$

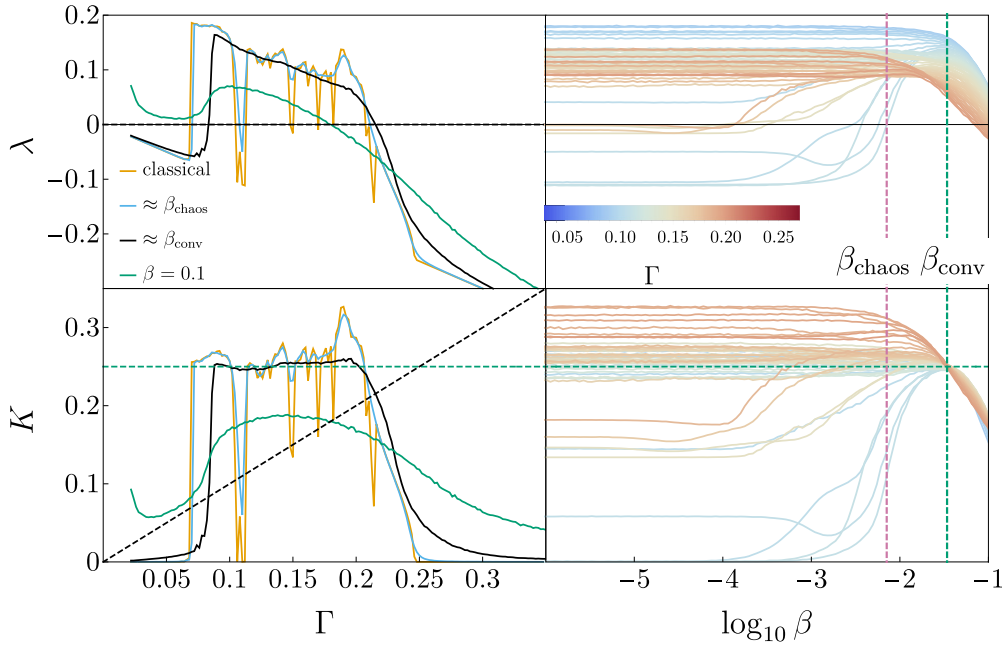


FIG. 2. The Lyapunov exponent (λ) and the dynamical complexity (K) as a function of dissipation Γ and system size β are shown. The right two plots focus on $0.088 < \Gamma \leq 0.2$. Both plots show that all classically periodic orbits become chaotic at $\beta = \beta_{\text{chaos}}$. Classically chaotic dynamics, in comparison, are robust as the length scales decreases. Note also that there is a convergence of the dynamical complexity at β_{conv} . This convergence is also confirmed using d in Fig. 5.

$$d\Pi = \left[\rho(-3\beta^2 x^2 + 1) + \frac{1}{4\rho^3} - \Gamma\Pi \left(1 + \Pi^2 + \rho^2 + \frac{3}{4\rho^2} \right) \right] dt. \quad (7)$$

The semiclassical model shows quantum features in three ways: (1) the influence of the spread variables ρ and Π on x , p , (2) the environmental coupling appearing via noise terms proportional to $2\sqrt{\Gamma}$ for dx and dp , and (3) a tunneling-like effect where the size of the barrier between the two wells of the x , p is proportional to $(1 - 3\beta^2\rho^2)$. The classical system is recovered from the semiclassical approximation by increasing the system size i.e., by letting $\beta \rightarrow 0$. This system can be understood as the x , p “centroid” oscillator coupled to the ρ , Π oscillator, with the latter two representing the wave packet spread, evolving with noise and dissipation in the potential [4]

$$U(x, \rho) = -(1 - 3\beta^2\rho^2)\frac{x^2}{2} + \beta^2\left(\frac{x^2}{2}\right)^2 - \left(\frac{g}{\beta}\cos\omega t\right)x - \frac{\rho^2}{2} + \frac{1}{8\rho^2} \quad (8)$$

that is also subject to noise and dissipation. In the remainder of the paper, we refer to this semiclassical model as “SC.”

Recall that Eq. (1) is β invariant other than a change in the length scales. Therefore, the natural scale of analysis is $x\beta$, $p\beta$. Under these “scaled” coordinates, the stochastic term in the semiclassical Eqs. (4) and (5) scale with β , while the tunneling term $1 - 3\beta^2\rho^2$ scales with β^2 . It is therefore likely that the initial effect of increasing β away from the classical limit arises from the stochastic terms. To isolate the effect of noise, we create a third model based on SC by

fixing $\beta = 10^{-5}$ for the system—a length scale where the semiclassical dynamics differs only slightly from the classical Newtonian dynamics—except to allow for a scaling of the noise terms by a factor β_n so that $d\xi_{R,I} \rightarrow \beta_n d\xi_{R,I}$. We refer to this complex-noise added classical model as “C + $\mathcal{N}_{\mathbb{C}}$.” The hypothesis about the dominant role of the environment suggests that varying β_n for C + $\mathcal{N}_{\mathbb{C}}$ should reproduce the effect of varying β for SC until we reach the smallest length scales. This immediately raises the question of whether a Gaussian noise-added classical model can reproduce the semiclassical dynamics without having to consider the semiclassical dynamics at all. To this end we consider the Duffing oscillator with a noise term $2\sqrt{\Gamma}d\xi$ added to the classical Duffing equations, resulting in

$$dx = p dt + 2\sqrt{\Gamma} d\xi, \quad (9)$$

$$dp = -\beta^2 x^3 + x - 2\Gamma p + \frac{g}{\beta} \cos(\omega t) dt + 2\sqrt{\Gamma} d\xi. \quad (10)$$

This real-noise added model is referred to as C + $\mathcal{N}_{\mathbb{R}}$.

Having established the various models of increasing complexity we use, we now turn to the metrics used to characterize the dynamics. The standard tool for characterizing complex dynamics measures the sensitivity to initial conditions is the largest Lyapunov exponent (λ) which distinguishes chaotic ($\lambda > 0$) and periodic ($\lambda \leq 0$) dynamics [26]. We calculate λ using the canonical methods [27]. However, in the classical system, for POs at a given Γ we get $\lambda_{\text{PO}} = -\Gamma$. We therefore also use the previously introduced [10] dynamical complexity $K = \lambda + \Gamma$ quantifying how much more complex a given orbit is compared to the minimal case of a PO. K is strictly non-negative and compensates for the natural phase-space volume shrinkage caused by increasing dissipation Γ (see Fig. 2). As

a result, here K allows for an effectively binary classification of Duffing attractors (see Fig. 2) across β and Γ with complex chaotic attractors having $0.2 < K < 0.3$ and simple periodic attractors having $K < 0.2$, independent of Γ .

Despite their value and widespread use, Lyapunov exponents can miss dynamical nuances. In particular, the Lyapunov exponent quantifies the average temporal complexity and not the spatial complexity of the dynamics. A comparison of Poincaré sections for different semiclassical approximations shown in Fig. 1, can be informative in understanding spatial complexity differences. However, different stochastic terms [Eqs. (4) to (7)] “blur” the Poincaré sections differently albeit not always visually distinguishable. In other words, visual comparisons do not allow us to quantify the differences between dissimilar Poincaré sections, which would allow us to rank-order dissimilarity. To this end, we introduce a Kullback-Leibler inspired spatial similarity metric d that allows us to compare different phase-space Poincaré sections. In particular, for two histogram distributions $f_1(x)$ and $f_2(x)$, the distance l [18] is defined as

$$l(f_1, f_2) = -\ln \left[\frac{\int [f_1(x)f_2(x)]^2 dx}{[\int f_1(x)f_1(x) dx][\int f_2(x)f_2(x) dx]} \right]. \quad (11)$$

Given a dynamical model M (semiclassical or noise-added classical), we compute the l over each coordinate of the phase space and take the Eulerian sum

$$d_{M_1, M_2}(\Gamma_1, \beta_1; \Gamma_2, \beta_2) = \sqrt{\sum_{j \in \{x, p\}} l[M_1^j(\Gamma_1, \beta_1), M_2^j(\Gamma_2, \beta_2)]^2}, \quad (12)$$

where M^j is the coarse-grained Poincaré-section histogram for the j th phase-space coordinate. Note that we do not consider the coordinates ρ , Π as they are only defined for SC and $C + \mathcal{N}_C$. Two identical Poincaré sections yield $d = 0$ and two orthogonal sections yield $d \rightarrow \infty$. This distance is only well defined for chaotic trajectories; for periodic trajectories, the distributions are too localized and even slight differences can lead to large distances (see Appendix B for more details).

III. RESULTS AND DISCUSSION

At the classical limit, the Duffing oscillator has a standard and rich transition between regularity and complexity as a function of most dynamical parameters. Changing the strength Γ of the coupling to the environment (which classically affects only the dissipation due to the environment and not fluctuations) also induces this behavior, including windows of periodic behavior and a regime of coexisting attractors [28]. This parametric sensitivity which leads to abrupt changes in dynamical behavior has potential consequences in metrology as well applications in quantum control [3]. Before mapping the details of how the variety of classical dynamics and the classical sensitivity to parameters behave under change of length scale, we first establish the value of independently analyzing temporal complexity (using λ) and spatial similarity (using d). To do this, consider a classically chaotic attractor at $\Gamma = 0.174$ and $\beta = \beta_{\text{conv}}$ under different approximations C , $C + \mathcal{N}_R$, and $C + \mathcal{N}_C$. In Fig. 1 we compute λ and the distance $d_{SC,x}$ for different semiclassical approximations. We find the following:

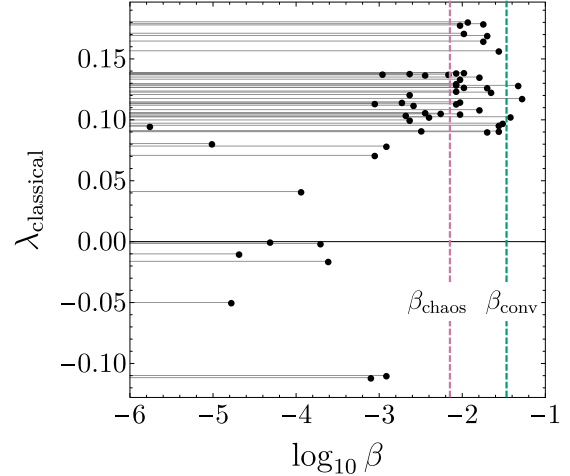


FIG. 3. β_{break} is the length scale at which $\lambda(\beta)$ diverges from the classical Lyapunov. β_{break} as a function of $\lambda_{\text{classical}}$ is shown.

(1) Phase-space attractors that look different [like Figs. 1(b) and 1(d)] are quantifiably more similar to each other in d than ones that at first appearance look similar [Figs. 1(a) and 1(d)].

(2) Statistical differences between the semiclassical (SC) and classical-noise added model ($C + \mathcal{N}_R$), which is missed by λ , do produce quantitatively and visually different spatial complex Poincaré sections [Figs. 1(b) and 1(d)].

(3) Even though the phase-space attractors for $C + \mathcal{N}_C$ and SC are visually nearly identical, there are differences that can be captured by both λ and d [Figs. 1(c) and 1(d)].

With these caveats in mind, consider the temporal complexities $\lambda(\Gamma)$ and $K(\Gamma)$. The Γ landscape can be divided classically into three regimes: low ($\Gamma < 0.068$), intermediate ($0.068 \leq \Gamma < 0.2$), and high ($\Gamma > 0.2$). For low damping, the orbits are regular orbits that traverse both wells of the Duffing oscillator; for high damping, owing to the overwhelming magnitude of Γ we observe single-well regular orbits.

Motivated by the inherent linearity of Hamiltonian quantum dynamics, it has been suggested that quantum mechanics makes systems more regular. Further, the timescale of emergence of quantum-classical differences are argued to scale with the Lyapunov exponent of the classical dynamics, with classically chaotic dynamics having maximal deviation from quantum behavior. However, in NQDS in general and Fig. 2 in particular, we see all four possible transitions as a function of β : regular-to-regular, regular-to-chaos, chaos-to-regular, and chaos-to-chaos. For example, the lower portion of the intermediate regime ($0.068 \leq \Gamma < 0.088$) shows a transition from classical chaos to semiclassical regularity. Here quantum effects delay the impact of increasing dissipation. Therefore, we see a “quantum regularization” of chaos and the increase in λ as a function of Γ gets shifted. Some of the interesting effects due to the existence of a coexisting attractor in this regime are discussed further in the Appendix E. The bulk of our analysis here, however, focuses on the intermediate regime $0.088 \leq \Gamma < 0.2$. Here we see chaos-to-chaos and regular-to-chaos transitions as a function of β .

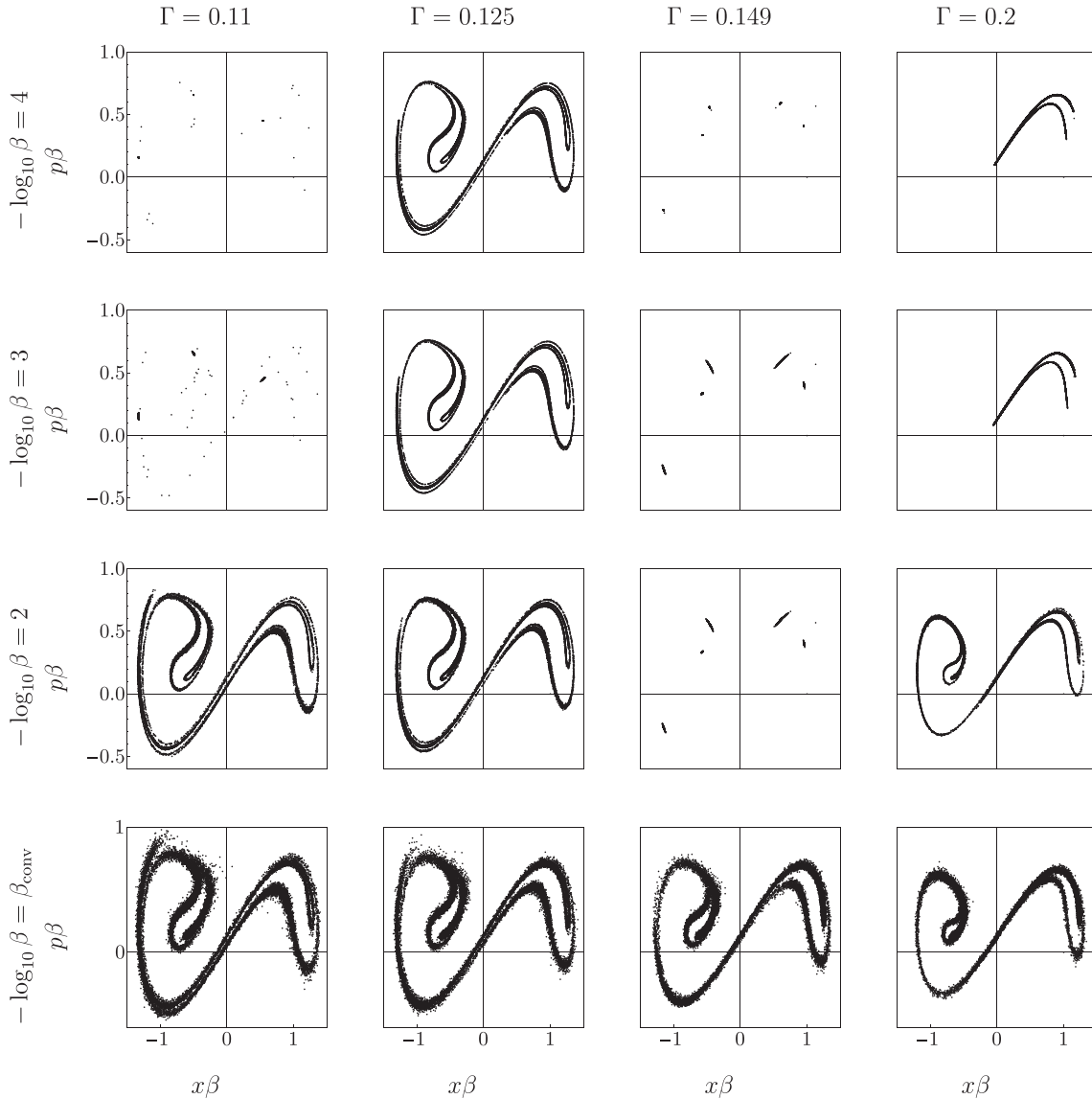


FIG. 4. Poincaré for attractors with coupling $\Gamma = 0.11, 0.125, 0.149, 0.2$ for length scales between $\beta = 0.00001$ and $\beta_{\text{conv}} = 0.0341$ generated using the SC model. As $\beta \rightarrow \beta_{\text{conv}}$, we see a chaotification of periodic orbits for $\Gamma = 0.11, 0.149$. Overall, the attractor become more similar to one another hence demonstrating the emergence of the meta-attractor.

Consider the behavior of temporal complexity as function of β in Figs. 2 and 3. As Pokharel *et al.* [10] previously noted, introducing more quantum effects (increasing β) decreases the parametric sensitivity of temporal complexities to Γ when compared to the classical system. This “chaotification” is evident in the smoothing of the jaggedness of $K(\Gamma)$ (where the jaggedness corresponds to dips of regularity arising from higher order POs) as we scan $\beta > \beta_{\text{classical}}$. This arises primarily because the addition of “quantum” terms to the classical equations quickly destroys the higher period POs, which rely on dynamical synchronization across many periods. Consequently, all periodic attractors for $\Gamma \in (0.088, 0.2]$ become chaotic for scales below $\beta_{\text{chaos}} = 0.0068$. Moreover, the temporal complexity curves $\lambda(\beta), K(\beta)$ are highly nonmonotonic and idiosyncratic as a function of β (see Fig. 2). This is a distinctive feature observed in NQDS.

It is intriguing to see in these results a β scale where a Γ -invariance in dynamical complexity emerges—that is, starting at β_{conv} and persisting for small range in β , all dynamical attractors are seen to have the same value of K independent of Γ . Note that λ and K both capture β -invariance, while only K captures that the complexity of the dynamics becomes independent of environmental coupling Γ at a certain length scale. To be more specific, at a particular degree of quantumness $\beta = \beta_{\text{conv}} = 0.0341$, $K(\Gamma)$ flattens. When we consider the Poincaré sections themselves in this regime (Fig. 4) we confirm this remarkable convergence in dynamical complexity in the spatial similarity between the phase-space attractors. Again, the quantitative analysis using K and D allows clarity on this issue compared to visually estimating when Poincaré sections have converged as in Fig. 4 where a few scattered points can be deceiving. In particular, in Fig. 5 we compute

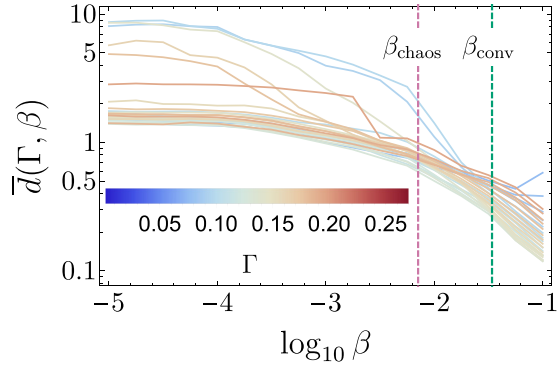


FIG. 5. The mean distance between a given oscillator at some Γ and all its counterparts in the range $[0.088, 0.2]$ is shown. Corroborating the observation in Fig. 2, this distance between all attractors is decreasing for all oscillators, with all attractors becoming indistinguishable from the meta-attractor as the length scale decreases.

the average distance between the attractor for a trajectory at Γ to all its counterparts in the range $\Gamma \in (0.088, 0.2]$ under the same model M and system size β

$$\bar{d}(\Gamma, \beta) = \text{mean}_{\Gamma'}(d_{M,M}(\Gamma, \beta; \Gamma', \beta)). \quad (13)$$

This average spatial similarity between attractors decreases as a function of system size. In other words, near β_{conv} both spatial and temporal complexity are invariant under changes in the environmental coupling.

We can also replot the temporal complexity K against the length scales where the classical dynamics no longer agrees with the semiclassical dynamics (i.e., β_{break}) in Fig. 3. In Fig. 3 we also see that not only is β_{break} lower for classical POs, implying that such behavior is harder to reproduce for a quantum system, but also that the break length scale is not intuitively related to the degree of chaos in the classical system $\lambda_{\text{classical}}$. This latter stands in contrast to the standard arguments about quantum “break time” that have persisted in the literature for many decades [29] but were constructed without considering the genuine quantum-classical correspondence obtained by considering the effect of decoherence via the environment.

To summarize, the competition between environmental effects and chaos is richest for $\beta_{\text{classical}} \leq \beta \leq \beta_{\text{conv}}$, the upper and lower boundaries of which have β and Γ invariant attractors, respectively. As we detail below, $C + \mathcal{N}_{\mathbb{C}}$ closely mirrors semiclassical dynamics for systems larger than β_{conv} , which means that this range of scales is where noise from environmental coupling plays a significant role. At the same time, other than qualitative differences in how classically chaotic and regular orbits behave as a function of system size, there is no clear connection between the degree of classical chaos and quantum-classical deviation. We also see evidence for a chaotic attractor with β and Γ invariant dynamical and spatial complexity which is what we have termed a “meta-attractor.”

We now turn from individual behavior to global characterization of various models. To do this, we compare the dynamics under different models by averaging distances over different parameters. In particular, we define a measure of the distance between two different models M_1 and M_2 at some

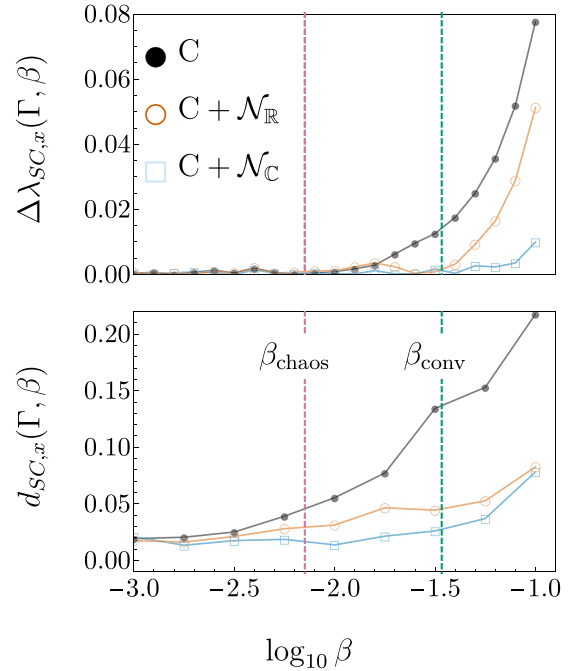


FIG. 6. The change in difference between semiclassical approximations as a function of system size as captured by $\Delta \lambda$ and d . The oscillator chosen is the central oscillator, which has $\Gamma = 0.138$. For this Γ both metrics show a monotonic increase in the difference as the system size gets smaller and quantum effects become more prominent. However, the difference in dynamics at larger system sizes is more visible in d than in λ . In other words, there exist length scales (for instance $\beta = \beta_{\text{chaos}}$) for which approximate models do not reproduce the spatial attractor, even though the Lyapunov exponent is reproduced.

specified system size β and averaged over a range of Γ as

$$\bar{d}_{M_1, M_2}(\beta) = \text{mean}_{\Gamma}(d_{M_1, M_2}(\Gamma, \beta; \Gamma, \beta)). \quad (14)$$

An equivalent similarity metric can also be defined for comparing temporal complexity

$$\bar{\Delta \lambda}_{M_1, M_2}(\beta) = \text{mean}_{\Gamma}(|\lambda_{M_1}(\Gamma, \beta) - \lambda_{M_2}(\Gamma, \beta)|). \quad (15)$$

We start with a typical case of a classically chaotic attractor at $\Gamma = 0.138$ in Fig. 6. Here we see that (1) all of the approximations to the accurate semiclassics get monotonically worse as the system size decreases, (2) as we increase the number of semiclassical terms, the difference between the noise-added models and the semiclassical model decreases i.e., that $C + \mathcal{N}_{\mathbb{C}}$ does better than $C + \mathcal{N}_{\mathbb{R}}$, and (3) comparing the top and the bottom figures, we notice that even when the Lyapunov exponents under different models are identical, for instance at β_{chaos} , the underlying attractors might not be spatially similar. As we discuss below, points (2) and (3) remain true in general for both classically chaotic and regular oscillators, but (1) need not.

This simplicity does not persist in the aggregate behavior shown in Fig. 7. Here the figures in third column are averaged over all Γ in the range $(0.088, 0.2]$ and are the weighted sum of the first two columns, which are over the classically chaotic and periodic trajectories respectively. The aggregate behavior looks far more structured and to understand this structure, we

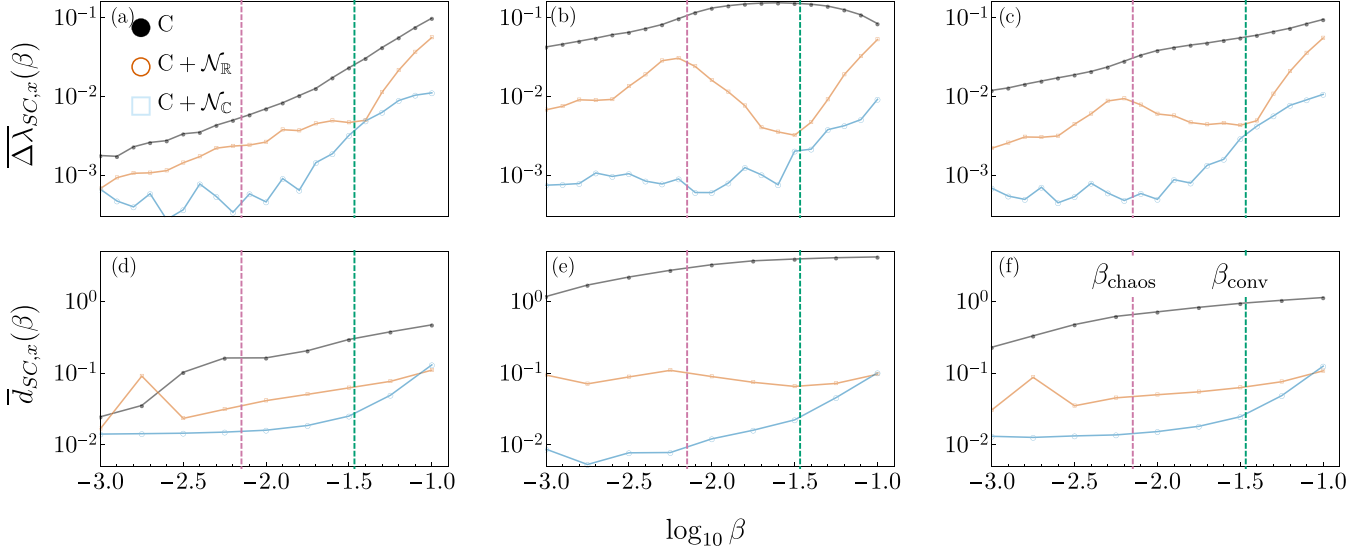


FIG. 7. $\Delta\lambda$ and d shown as a function of length scale β , while averaged over various Γ ranges. (a) and (d) consider classically chaotic Γ , (b) and (e) consider classically periodic Γ , and (c) and (f) consider the average over all Γ . Even though different approximations to the semiclassical are visually (in terms of Poincaré sections) and qualitatively similar to the full semiclassical model, the difference between the models can be quantified. Just like Fig. 6, both difference measures are monotonic in (a) and (d) for classically chaotic attractors, other than an anomalous peak at $\log_{10} \beta = -2.75$ (see Appendix B for more details). On the other hand, classically periodic orbits are the hardest to recover using approximate semiclassics: the nonmonotonic behavior of $\Delta\lambda$ over the entire range of Γ is due to the classically periodic orbits in (b) and (e). The differences $\Delta\lambda$ and d between the semiclassical and noise-added classical models is the highest at $\beta = \beta_{\text{chaos}}$, after which all oscillators become chaotic. At $\beta = \beta_{\text{conv}}$, noise washes out the differences between different oscillators leading to the convergence shown in Figs. 2 and 5; and all the approximate semiclassical models lose relevance for $\beta < \beta_{\text{conv}}$.

first note that the rapid fluctuation in $\overline{\Delta\lambda}(\beta)$ for $C + \mathcal{N}_C$ are of the order 10^{-3} which are inherent numerical precision errors arising from how the Lyapunov exponents are computed and further visually amplified by the log scale. Apart from the overall increasing deviation of noise-added models from the semiclassical model SC as a function of β , there are several nonmonotonic features which we now discuss.

The nonmonotonicity of $\overline{\Delta\lambda}(\beta)$ for the overall average behavior in Fig. 6(c) is due to the classical POs, as clearly seen in Fig. 6(b). The peak of $\Delta\lambda$ near β_{chaos} in Fig. 6(b) highlights the sensitivity of classical POs to Gaussian noise as this sensitivity drops when all trajectories are chaotic for $\beta > \beta_{\text{chaos}}$. Put differently, the semiclassical behavior of classical POs is harder to estimate using classical-noise added models and consequently requires the more sophisticated dynamical description given by $C + \mathcal{N}_C$ and SC.

The nonmonotonicity in $\overline{d}(\beta)$ is largely due to an anomalous peak at $\log_{10} \beta = -2.75$, most visible in Figs. 6(d) and 6(f). At this β -value, we see a single-well chaotic attractor in the noise-added models, which is spatially different from the true semiclassical double-well attractor (see Appendix B for more details). This peak in $\overline{d}(\beta)$ is not picked up by the Lyapunov exponents. Overall, we find that the spatial metric measuring the difference between phase-space attractors, d , does better at distinguishing between different models than λ . This emphasizes the need to use both spatial and temporal complexity metrics separately to study NQDS. Even when averaged, we see that spatial and temporal similarity of the models to the semiclassical dynamics gets progressively better as we use more sophisticated approximations. Moreover, for $\beta < \beta_{\text{conv}}$ the $C + \mathcal{N}_C$ model approximates the semiclassical

model well. This close similarity between SC and $C + \mathcal{N}_C$ suggests that increased sensitivity to the environment is the dominant mechanism by which quantum effects manifest in this NQDS.

IV. CONCLUSION

Nonlinear quantum dissipative systems evolve under an interplay between quantum effects, noise, and nonlinearity. Our exploration of the quantum-classical transition in an NQDS, in particular a noisy nonlinear driven oscillator, shows several interesting features. We have demonstrated that while Lyapunov exponents and visual examinations of the phase space Poincaré sections provide a reasonable first gauge of change in dynamical complexity or attractor similarity across systems, more careful metrics such as the dynamical complexity K and a distance measure between phase-space attractors d and their averages provide a better and more nuanced insights about this transition.

We have also investigated whether the semiclassical dynamics here can be explained by simply adding classical noise. We find that while classical noise produces certain qualitative features, there are spatial and temporal quantitative features that require taking quantum effects into account. In comparing across different dissipation models we see that indeed they get more accurate as the complexity of the model is increases. This monotonicity in resource complexity highlights the need for more complex models in noisy situations. We also find that the phenomenon of meta-attractors and of noise washing out POs is not dependent on the noise model used. Consequently, transitions from POs to chaos happens in

every model, and even the addition of simple Gaussian noise can make classically periodic orbits act in unexpected ways. As a result, semiclassical POs are not necessarily parametrically stable, but chaotic attractors are robust to noise and therefore model choice.

Surprisingly, the length scale for the breakdown of classical approximations to quantum behavior is not determined by the degree of classical chaos in the system, and the growth of quantum-classical difference is in general quite idiosyncratic. Thus, classically periodic and uncomplicated physical behavior can necessitate complicated and resource-intensive description in the semiclassical regime. Such semiclassical techniques have been studied and used widely over the decades, particularly in chemical physics [30–32]. Understanding what precisely does determine the break length scale remains of great interest as an avenue for future work. Further, we find that smaller, more “quantum” systems have few complicated periodic orbits due to increased sensitivity to environmental fluctuations. They are thus less sensitive to parameter variation than their classical counterparts. Remarkably, this leads to a chaotic meta-attractor fairly deep in the quantum regime that exhibits the same dynamical complexity independent of the environmental coupling and varying little qualitatively with length scale.

Such experimental systems are currently within reach: the quantum Duffing oscillator and the corresponding nonlinear behavior has been investigated for nanoelectromechanical systems by Li *et al.* [6] and for optomechanical devices [33], which has been recently further developed by Shi *et al.* [34]. Moreover, Peano and Thorwart [35] have discussed the possibility of implementing this oscillator in a superconducting qubit system. These experimental systems could be used to test the behavior described in this paper. Arguably, even our most sophisticated semiclassical model, which implicitly uses an environment consisting of a Markovian bath at zero temperature, remains relatively simple. In particular, considering a finite bath at a finite temperature with manifestly non-Markovian features would allow for richer investigation of NQDS. Analyzing how features of the current analysis are altered by different, more sophisticated noise spectra, is another obvious next challenge. Given these and related questions, the semiclassical regime of NQDS remains an intriguing area for further exploration.

ACKNOWLEDGMENTS

We would like to thank Bruce Duffy for computational support. B.P. would like to thank Namit Anand for insightful discussions. A.P. is grateful for HHMI funding through Carleton and internal funding from Carleton for student research. The authors would like to acknowledge useful and helpful feedback from anonymous referees.

A.D.M. and B.P. contributed equally to this work.

APPENDIX A: DERIVATION OF THE FOUR-EQUATION SEMICLASSICAL MODEL

The dissipative dynamics of the open semiclassical Duffing oscillator results in a conserved quantity, corresponding to reducing the wave function to one which is a minimum

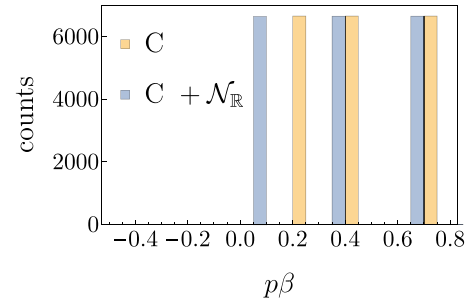


FIG. 8. Although the C and $C + \mathcal{N}_R$ models have almost identical Lyapunov exponent and similar spatial behavior as apparent in this plot, the distance measure d fails to capture the similarities between distributions where the peaks in the distributions are offset by small amounts.

uncertainty wave packet. This enables the five-equation semiclassical Duffing oscillator model from [10] to be reduced to four equations. To be more explicit, consider

$$dx = p dt + 2\sqrt{\Gamma} \left[\left(\mu - \frac{1}{2} \right) d\xi_R - R d\xi_I \right], \quad (\text{A1})$$

$$dp = \left(-\beta^2(x^3 + 3\mu x) + x - 2\Gamma_p + \frac{g}{\beta} \cos \omega t \right) dt + 2\sqrt{\Gamma} \left[R d\xi_R - \left(\kappa - \frac{1}{2} \right) d\xi_I \right], \quad (\text{A2})$$

$$d\mu = \left[2R + 2\Gamma \left(\mu - \mu^2 - R^2 + \frac{1}{4} \right) \right] dt, \quad (\text{A3})$$

$$d\kappa = \left[2R(-3\beta^2 x^2 + 1) + 2\Gamma \left(-\kappa - \kappa^2 - R^2 + \frac{1}{4} \right) \right] dt, \quad (\text{A4})$$

$$dR = [\mu(-3\beta^2 x^2 + 1) + \kappa - 2\Gamma R(\mu + \kappa)] dt. \quad (\text{A5})$$

The minimum uncertainty condition that allows for this reduction is

$$\mu\kappa - R^2 = \frac{1}{4}. \quad (\text{A6})$$

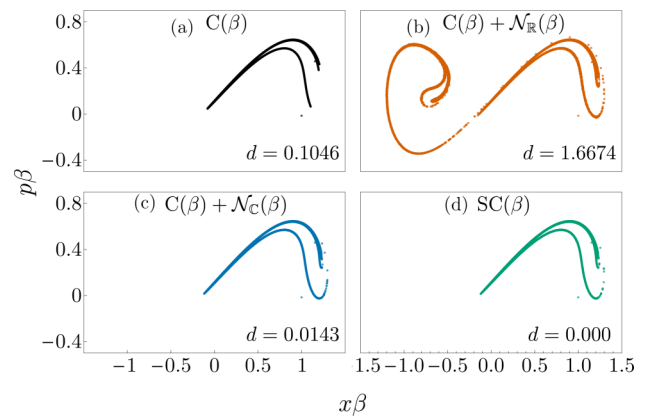


FIG. 9. Different approximations are compared to the semiclassical model at the cusp of a transition from single to double well orbits at $\Gamma = 0.174$, $\log_{10} \beta = -2.75$.

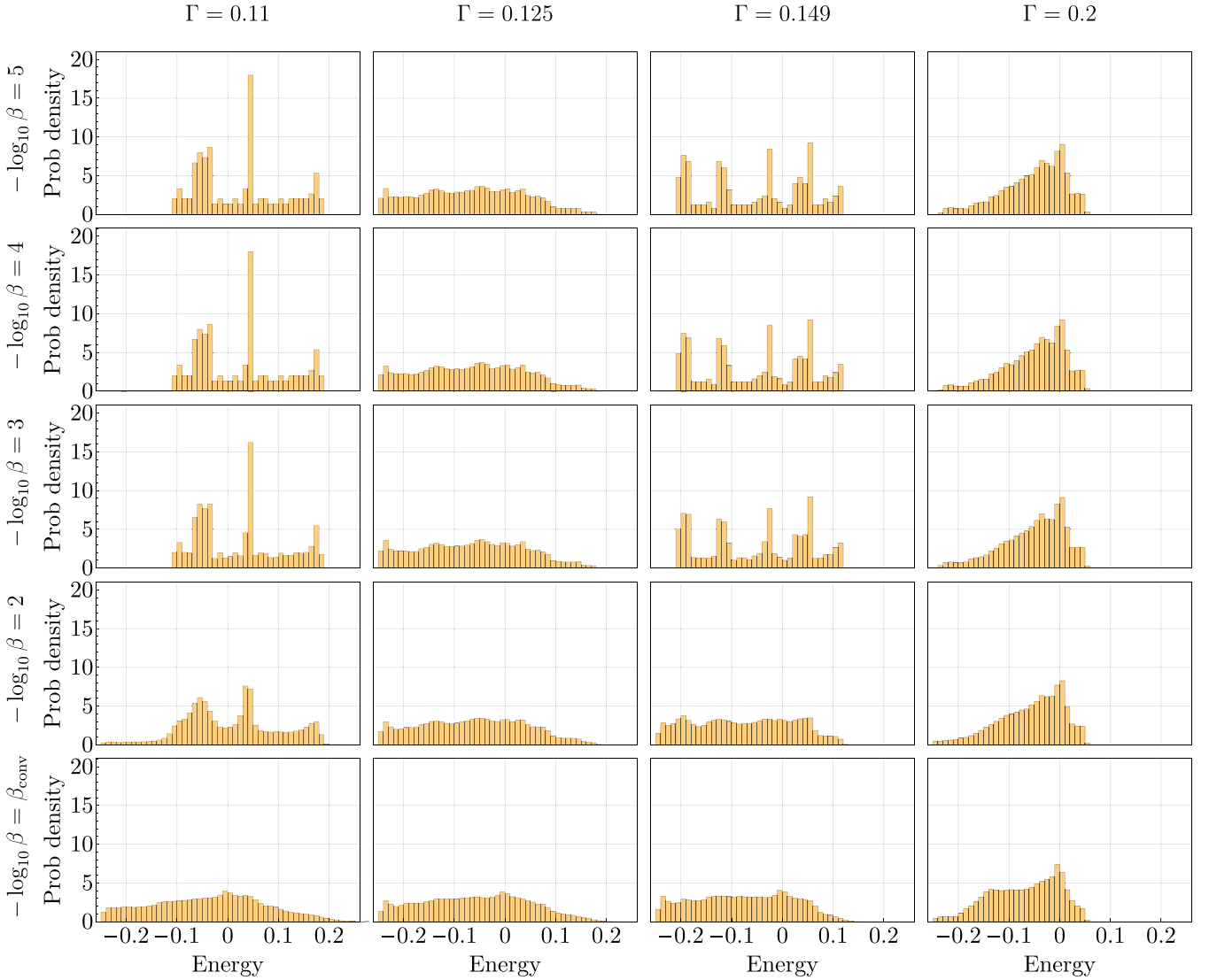


FIG. 10. Energy spectra for attractors with coupling $\Gamma = 0.11, 0.125, 0.149, 0.2$ for length scales between $\beta = 0.00001$ and $\beta_{\text{conv}} = 0.0341$. As $\beta \rightarrow \beta_{\text{conv}}$, the spectra become more similar to one another.

The time derivative of $\mu\kappa - R^2$ can be shown to be of the form $\dot{X} = -2\Gamma(\mu + \kappa)X$ and this guarantees the minimum uncertainty condition is quickly met when $2\Gamma(\mu + \kappa) > 0$ and $t \gg 1/2\Gamma(\mu + \kappa)$. We empirically confirm that the convergence is rapid. We then eliminate κ by

$$\kappa = \frac{R^2 + \frac{1}{4}}{\mu}. \quad (\text{A7})$$

We make two changes of variables: $\mu = \rho^2$ and $R = \rho\Pi$ [36]. It can be shown with Eq. (A7) that Eq. (A3) becomes

$$d\rho = \left[\Pi + \Gamma \left(\rho - \rho^3 - \rho\Pi^2 + \frac{1}{4\rho} \right) \right] dt. \quad (\text{A8})$$

We use $R = \rho\Pi$ and Eq. (A5) to show that

$$\begin{aligned} dR &= \Pi d\rho + \rho d\Pi \\ &= ([\mu(-3\beta^2 x^2 + 1) + \kappa - 2\Gamma R(\mu + \kappa)]) dt. \end{aligned} \quad (\text{A9})$$

Using $d\rho/dt$ and κ , we determine

$$\begin{aligned} d\Pi &= \left[\rho(-3\beta^2 x^2 + 1) + \frac{1}{4\rho^3} \right. \\ &\quad \left. - \Gamma\Pi \left(1 + \Pi^2 + \rho^2 + \frac{3}{4\rho^2} \right) \right] dt. \end{aligned} \quad (\text{A10})$$

Note that in the absence of environmental coupling ($\Gamma = 0$), this system corresponds to an x -oscillator coupled to an ρ -oscillator [36] with potential

$$\begin{aligned} U(x, \rho) &= -\frac{x^2}{2} + \beta^2 \left(\frac{x^2}{2} \right)^2 - \left(\frac{g}{\beta} \cos \omega t \right) x \\ &\quad - \frac{\rho^2}{2} + \frac{1}{8\rho^2} + \frac{3}{2}\beta^2(x\rho)^2. \end{aligned} \quad (\text{A11})$$

APPENDIX B: CAUSES OF DIVERGENCE IN d

We note that the distance metric d can yield meaningless results when comparing periodic attractors. This metric com-

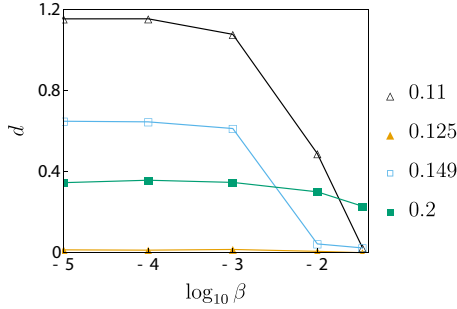


FIG. 11. The distance between the energy spectra in Fig. 11 and the spectra of $\Gamma = 0.125$ at β_{conv} . The distance decreases as $\beta \rightarrow \beta_{\text{conv}}$.

compares the distributions in x and p , meaning that even slight displacements in sparse distributions will cause the metric to diverge. An example of this is shown in Fig. 8. The models C and $C + \mathcal{N}_{\mathbb{R}}$ are quite similar and have nearly equal λ , but the distance $d = 18.5454$ is really large. This pattern is repeated in other examples of distances measured between periodic trajectories. For this reason, the lower bound of plots in Fig. 6 from the main text is set at $\log_{10}(\beta) = -3$, above the largest length scale at which this anomaly is present in the result.

The distance metric also fails in the vicinity of discontinuous changes of spatial behavior. The anomalous spike in $\Delta \bar{d}_{\text{SC}, C + \mathcal{N}_{\mathbb{R}}}$ at $\log_{10} \beta = -2.75$ [see Fig. 6(d) and 6(f)] is caused by a single attractor, $\Gamma = 0.198$, on the cusp of a transition from a single- to double-well orbit. This is evident in Fig. 9, where the Poincaré sections of C , $C + \mathcal{N}_{\mathbb{R}}$, and SC show trajectories constrained to the $+x$ well while the Poincaré section of $C + \mathcal{N}_{\mathbb{C}}$ shows a trajectory in both the $+x$ and $-x$ wells. The $C + \mathcal{N}_{\mathbb{C}}$ model jumps the gun on the discontinuous change from single to double well trajectories, resulting an anomalously high distance to SC.

APPENDIX C: ENERGY SPECTRA ANALYSIS

The convergence of attractors in the semiclassical regime is also evident in energy spectra. Figure 10 shows energy spectra for attractors with coupling $\Gamma = 0.11, 0.125, 0.149, 0.2$ for length scales between $\beta = 0.00001$ and $\beta_{\text{conv}} = 0.0341$. Note that attractors ($\Gamma = 0.125, 0.2$) are classically chaotic and ($\Gamma = 0.11, 0.149$) are classically periodic. These attractors are generally representative of energy spectra in the intermediate coupling regime. The spectra are increasingly similar as $\beta \rightarrow \beta_{\text{conv}}$, although $\Gamma = 0.2$ at the edge of the intermediate coupling regime is not as converged as the others. We quantify this convergence by measuring the distance d between the given spectra and the spectra of $\Gamma = 0.125$ at β_{conv} (see Fig. 11). As expected, the distance decreases as β increases, illustrating a convergence of attractors.

APPENDIX D: CLASSICAL NOISE-ADDED MODELS

Figure 12 shows $K(\beta; \Gamma)$ for $C + \mathcal{N}_{\mathbb{R}}$, $C + \mathcal{N}_{\mathbb{C}}$, and SC in the intermediate coupling regime. While the qualitative behavior of the classical noise added models is similar to SC, there are noticeable differences as highlighted in the main text. The variation between the models is more pronounced as $\log_{10} \beta$ increases past $\log_{10} \beta_{\text{conv}}$. We note that the K convergence is not unique to the SC model. The convergence in K can be caused by simply adding classical noise to the Duffing oscillator as well; it does not require a quantum description.

APPENDIX E: DUFFING OSCILLATOR BEHAVIOR IN LOWER AND HIGHER ENVIRONMENTAL COUPLING REGIMES

We present our investigation of lower and higher coupling regimes here for the sake of completeness. In the low coupling regime, $\Gamma < 0.068$, we observe $\lambda = -\Gamma$ in classical and most

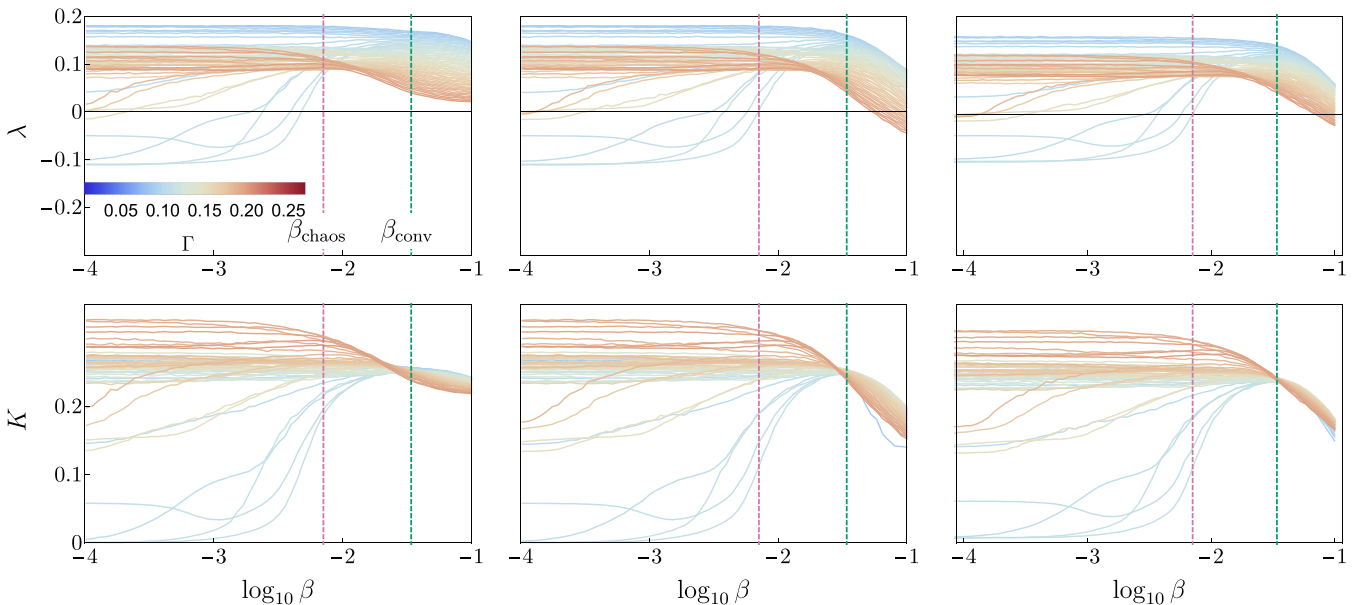


FIG. 12. Each column represents the $\lambda(\beta; \Gamma)$ and $K(\beta; \Gamma)$ curves for the two classical noise-added models ($C + \mathcal{N}_{\mathbb{R}}$ and $C + \mathcal{N}_{\mathbb{C}}$) and the semiclassical model (SC). Γ is set to be in the intermediate damping regime ($0.088 \leq \Gamma < 0.202$).

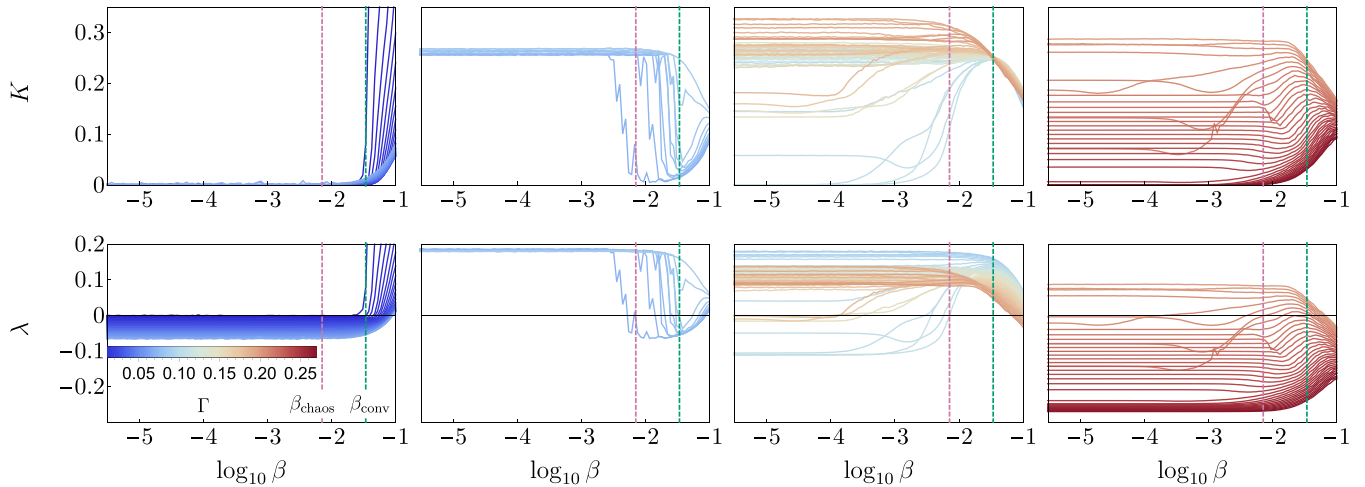


FIG. 13. The top row of subplots show λ as a function of length scale $[\log_{10}(\beta)]$ for the semiclassical model over four ranges of increasing Γ that correspond to distinct regions of behavior for λ and K . The bottom row shows the same ranges of Γ values for K as a function of length scale, $\log(\beta^{-1})$.

semiclassical length scales, as seen in Fig. 13. The oscillator traverses both wells in single period orbits. At high β , we observe a rise in λ that aligns with the “chaotification” of low coupling periodic orbits discovered earlier [10]. However, these values of both small Γ and large β are beyond the range of validity of the semiclassical formalism, and we do not attribute any physical meaning to this rapid change in λ .

Between the low and intermediate coupling regimes ($0.068 \leq \Gamma < 0.088$), classically chaotic orbits sharply transition to periodic behavior at some semiclassical length scale $-3 < \log_{10} \beta < \log_{10} \beta_{\text{conv}}$ (see Fig. 13). During the transition from chaotic to periodic behavior, the oscillator gradually localizes to a single well and a double-peaked, high-energy cluster emerges in the energy spectra (see Fig. 14). We suspect

that (1) the POs at high β in this coupling regime are linked to the classical POs in the low coupling regime and (2) the chaotic orbits at low β are linked to the classical chaotic orbits in the intermediate regime. Given that previous work has shown that the Lyapunov exponent is sensitive to initial conditions for some attractors in this regime [28], further exploration is warranted. The overall effect of this phenomena is that increasing β results in a delay to the onset of chaos with respect to coupling Γ . In the high coupling regime ($\Gamma > 0.2$), λ falls off steeply with higher Γ . Here the oscillator is increasingly limited to a single well because of heavy dissipation through the environmental coupling. For $\Gamma \geq 0.25$, the oscillator obeys $\lambda = -\Gamma$ for much of the semiclassical regime. Similar to the low coupling regime, λ monotonically rises at sufficiently large β .

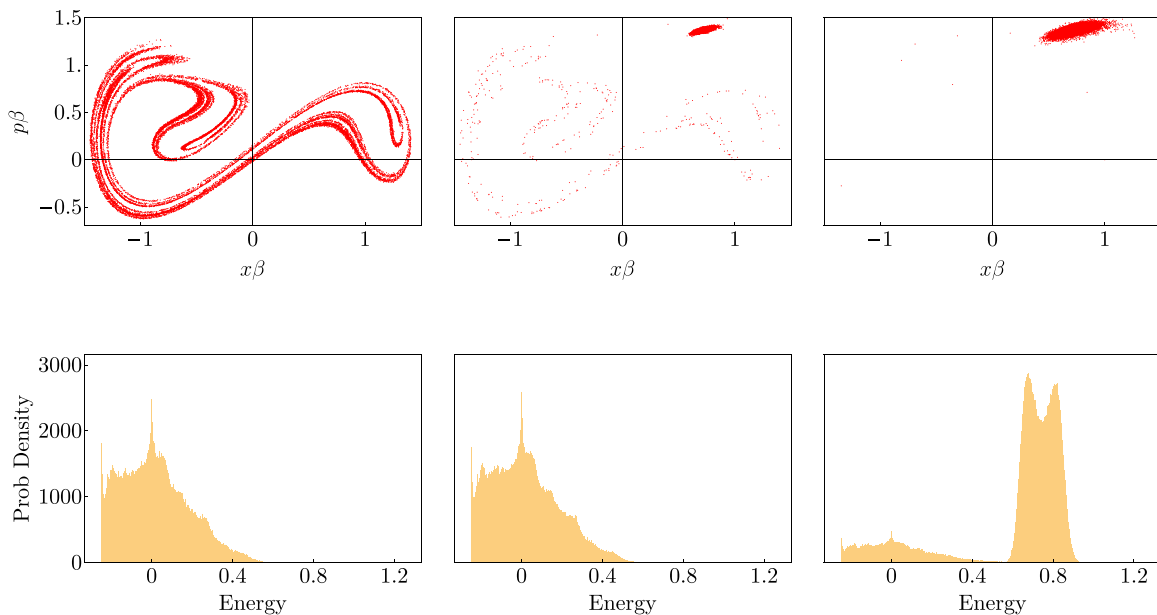


FIG. 14. An example of the transition between chaotic and periodic motion for coupling levels between the low and intermediate range visualized with energy spectra and Poincaré sections. Attractors in this range ($0.068 \leq \Gamma < 0.88$) all exhibit a similar transition.

- [1] K. Jacobs and A. J. Landahl, *Phys. Rev. Lett.* **103**, 067201 (2009).
- [2] J. Preskill, *Quantum* **2**, 79 (2018).
- [3] J. K. Eastman, J. J. Hope, and A. R. R. Carvalho, *Sci. Rep.* **7**, 44684 (2017).
- [4] Y. Shi, S. Greenfield, J. Eastman, A. Carvalho, and A. Pattanayak, in *Proceedings of the 5th International Conference on Applications in Nonlinear Dynamics*, edited by V. In, P. Longhini, and A. Palacios (Springer, 2019), pp. 72–83.
- [5] L. Bakemeier, A. Alvermann, and H. Fehske, *Phys. Rev. Lett.* **114**, 013601 (2015).
- [6] Q. Li, A. Kapulkin, D. Anderson, S. Tan, and A. Pattanayak, *Phys. Scripta* **T151**, 014055 (2012).
- [7] J. Larson and D. H. J. O’Dell, *J. Phys. B: At. Mol. Opt. Phys.* **46**, 224015 (2013).
- [8] T. Bhattacharya, S. Habib, and K. Jacobs, *Phys. Rev. Lett.* **85**, 4852 (2000).
- [9] S. Ghose, P. Alsing, I. Deutsch, T. Bhattacharya, and S. Habib, *Phys. Rev. A* **69**, 052116 (2004).
- [10] B. Pokharel, M. Z. R. Misplon, W. Lynn, P. Duggins, K. Hallman, D. Anderson, A. Kapulkin, and A. K. Pattanayak, *Sci. Rep.* **8**, 2108 (2018).
- [11] I. I. Yusipov, O. S. Vershinina, S. Denisov, S. P. Kuznetsov, and M. V. Ivanchenko, *Chaos* **29**, 063130 (2019).
- [12] J. F. Ralph, K. Jacobs, and M. J. Everitt, *Phys. Rev. A* **95**, 012135 (2017).
- [13] E. Ott, T. M. Antonsen, and J. D. Hanson, *Phys. Rev. Lett.* **53**, 2187 (1984).
- [14] T. Dittrich and R. Graham, *Europhys. Lett.* **4**, 263 (1987).
- [15] B. Klappauf, W. Oskay, D. Steck, and M. Raizen, *Phys. Rev. Lett.* **81**, 1203 (1998).
- [16] B. Klappauf, W. Oskay, D. Steck, and M. Raizen, *Phys. Rev. Lett.* **82**, 241 (1999).
- [17] H. Ammann, R. Gray, I. Shvarchuck, and N. Christensen, *Phys. Rev. Lett.* **80**, 4111 (1998).
- [18] A. K. Pattanayak, B. Sundaram, and B. D. Greenbaum, *Phys. Rev. Lett.* **90**, 014103 (2003).
- [19] J. Gong and P. Brumer, *Annu. Rev. Phys. Chem.* **56**, 1 (2005).
- [20] S. Habib, K. Shizume, and W. H. Zurek, *Phys. Rev. Lett.* **80**, 4361 (1998).
- [21] A. Kapulkin and A. K. Pattanayak, *Phys. Rev. Lett.* **101**, 074101 (2008).
- [22] I. Percival, *Quantum State Diffusion* (Cambridge University Press, Cambridge, 1998).
- [23] T. Brun, I. Percival, and R. Schack, *J. Phys. A* **29**, 2077 (1996).
- [24] Y. Ota and I. Ohba, *Phys. Rev. E* **71**, 015201(R) (2005).
- [25] J. Halliwell and A. Zoupas, *Phys. Rev. D* **52**, 7294 (1995).
- [26] G. Boffetta, M. Cencini, M. Falcioni, and A. Vulpiani, *Phys. Rep.* **356**, 367 (2002).
- [27] A. Wolf, J. Swift, H. Swinney, and J. Vastano, *Physica D* **16**, 285 (1985).
- [28] M. Z. R. Misplon and A. K. Pattanayak, (unpublished).
- [29] G. P. Berman and G. M. Zaslavsky, *Physica A* **91**, 450 (1978).
- [30] O. V. Prezhdo, *J. Chem. Phys.* **117**, 2995 (2002).
- [31] S. Tomsovic and E. J. Heller, *Phys. Rev. Lett.* **67**, 664 (1991).
- [32] D. Banerjee, B. C. Bag, S. K. Banik, and D. S. Ray, *J. Chem. Phys.* **120**, 8960 (2004).
- [33] G. J. Milburn and C. A. Holmes, *Phys. Rev. A* **44**, 4704 (1991).
- [34] Y. Shi, S. Greenfield, and A. K. Pattanayak, *Phys. Rev. A* **103**, 052212 (2021).
- [35] V. Peano and M. Thorwart, *Chem. Phys.* **322**, 135 (2006).
- [36] A. Pattanayak and W. Schieve, *Phys. Rev. E* **50**, 3601 (1994).